Journal of
Applied and Computational Mechanics

Shahid Chamran
University of Ahvaz

Research Paper

Magnetohydrodynamic Bio-convective Casson Nanofluid Flow: A Numerical Simulation by Paired Quasilinearisation

Md.S. Ansari[1], O. Otegbeye[2], M. Trivedi[1], S.P. Goqo[2]

[1] Department of Mathematics, School of Technology, Pandit Deendayal Petroleum University, India

[2] School of Mathematics, Statistics and Computer Science, University of KwaZulu-Natal, South Africa

Abstract. A study on the effects of gyrotactic microorganism and nanoparticles in the bio-convection magnetohydrodynamic flow of Casson fluid at the nonlinear stretching boundary is investigated. Irregular heat source/sink, Joule and viscous dissipations, Brownian motion, and thermophoresis are included in the energy equation. The model outlining the flow system is non-dimensionalised and retained in the same form. The equations are worked out by pairing, i.e. first pair momentum and gyrotactic micro-organism density equation and second pair energy and nanoparticle concentration equation. This technique is termed as a paired quasilinearisation method (PQLM). Convergence and accuracy of PQLM are shown. Obtained numerical results are depicted in graphs in order to observe further insight into the flow pattern. Interesting aspects of various controlling parameters in flow, heat, nanoparticle concentration and microorganism density are discussed.

Keywords: Casson nanofluid, Magnetic field, Nonlinear stretching sheet, Gyrotactic microorganism, Paired quasi-linearisation method.

1. Introduction

Conventionally, Non-Newtonian fluids have been used for various thermal convection processes widely appearing in different engineering applications like drilling mud used in construction of wellbores for oil and/or gas recovery, coating, printing and painting processes, polymeric fluid extrusion, plastic manufacturing processes, processing of food products, plastic film production using aerodynamic extrusion, annealing, shaping and thinning of various metal compounds like copper, aluminum, etc. The mechanics involving non-Newtonian fluid flow turns out to be a challenging task for engineers, physicists, and mathematicians. Due to the complexity in stress and strain relationship of non-Newtonian fluids, constitutive equations are not unique. Various models exist in literature characterizing different stress and strain relationship. Of these, fluids of the viscoelastic type termed Casson fluid have been looked over extensively. In the studies [1-7], authors have explored various flow models for Casson fluid under various geometries and boundary conditions. Research papers [8-10] present analysis on heat flux governed by modified Fourier law on non- Newtonian fluid flow.

Nanofluids are widely studied, due to the high demand for efficient heat transfer fluid, as it demonstrates better thermal properties than that of the base fluid. Nanofluid exhibits excellent heat transfer characteristics [11]. It gives minimal clogging in flow passage, enhanced thermal conductivity, long-term stability, and homogeneity. The presence of nanoparticles, made of copper, gold, oxides, carbon nanotube etc. in the base fluid, showed a significant improvement in heat transfer capabilities and stability of suspensions [12]. A different aspect and flow properties of Casson nanofluid (like mixed convection, thermal radiation, chemical reaction, heat source/sink, magnetic field, Newtonian heating, Cattaneo-Christov heat flux, etc.) were explored in [13-19] under stretching boundary. Ijaz et al. [20] evaluated the Maxwell fluid flow over stretched boundary together with the effects of ferromagnetic nanoparticle, magnetic dipole and heat source and sink.

Alsabery et al. [21] applied a numerical algorithm known as FDM to study magnetohydrodynamic natural convection of a nanofluid in a cavity with a conductive inner block. Convective MHD nanofluid flow near the stretching surface along with nonlinear radiation and heat generation/absorption was examined by Lu et al. [22]. CuO nanoparticle migration in a porous complex-shaped hot wall enclosure with two temperature model along with the impact of Lorentz forces was studied by Sheikholeslami et al.[23]. 3D MHD convective heat flow without nanoparticle mass flux conditions of nanofluid at the exponentially stretched surface was scrutinized by Ramzan et al. [24]. Al_2O_3-H_2O nanofluid free convection under the impact of uniform magnetic forces through a permeable cubic enclosure with an ellipse-shaped obstacle was studied by Sheikholeslami et al. [25]. A consequence of elliptic hot source and radiation on MHD free convection in a porous domain saturated with nanofluid was surveyed by Nguyen-Thoi et al. [26].

A field of research on nanofluid bioconvection emerged following the study of Kuznetsov[27]. Concept of bioconvection (a phenomenon exhibiting the streaming patterns perceived in dense culture of free-moving organisms [28]) was initiated by James Henry Platt in 1961. The process of bioconvection deals with macroscopic fluid motion resulting due to a change in density caused

by collective moving of motile micro-organisms in the flow domain [29]. Self-propelled micro-organisms increase the density of the base fluid in a particular direction resulting in the bioconvection flow. Micro-organisms are categorized into three types, negative gravitaxis, gyrotactic micro-organisms and oxytactic or chemotaxis [30]. The displacement between the center of mass, buoyancy, negative gravity and oxygen concentration gradient causes bioconvective flow [31]. Presence of gyrotactic microorganisms in nanofluid boost mass transfer especially in micro-volume. The motion of motile micro-organisms is self-induced whereas that of nanoparticle is due to random movement (i.e. Brownian motion) and thermophoretic effect in nanofluid. Bioconvection i.e. contemporaneous interplay of nanoparticles, buoyancy forces and self-propelled microorganisms finds application in field of biomedical systems, bioconjugates, design of bio cells, bio microsystem, reduction of blood loss during surgeries [32], microbial enhanced oil recovery as microorganisms reduce the viscosity of crude oil [33, 34], geophysical phenomena like thermophiles, in which motile microorganisms move toward hot spring [35] and marine biology [36].

Following the novel study [27], a series of research papers [37-50] appeared in literature dealing bio convection nanofluid flow with gyrotactic microorganisms. Ali et al. [59] reported an analysis of the presence of gyrotactic micro-organisms in Maxwell nanofluid near a stretching surface combining the impacts of heat source/sink and magnetic field. Ramzan et al. [51] analysed the bio-convective flow of magnetized suspended carbon nanotubes based nanofluid with entropy generation closeby vertical cone considering Joule heating, chemical reaction, and solutal stratified boundary. Recently, Oyelakin et al. [52] performed a simulation on the effects of gyrotactic microorganisms, solute concentration-dependent nanofluid properties and non-linear radiation in flow of Casson nanofluid close to moving wedge.

Above mentioned research papers and exhaustive literature, survey reveals that the study comprising heat generation/ absorption, viscous and Joule effects, the interaction of motile microorganisms on bioconvection Casson nanofluid flow at nonlinear stretching boundary, has not been carried out so far. The present work attempts to analyze MHD convective Casson nanofluid flow past a nonlinear stretching sheet. The thermal field incorporates the effect of heat generation/absorption along with viscous and Joule effects. The novelty of present work is to analyze flow behavior due to the presence of gyrotactic motile microorganisms in Casson nanofluid under the impacts of non-uniform heat source/sink, viscous and Joule dissipations. The partial differential equations modeling the flow are nondimensionalised by implementing a set of transformations. We did the solution of nondimensionalised PDEs with spectral paired quasi linearisation method (PQLM). The effects of Brownian motion, thermophoresis, magnetic field, Eckert number, bio-convective Lewis number, bio-convective Peclet number, etc., on momentum, thermal, nanoparticle concentration and density of motile microorganisms field are analyzed by replicating the numerical results in graphical and tabular form. Physical interpretation and convergence of solution method are discussed.
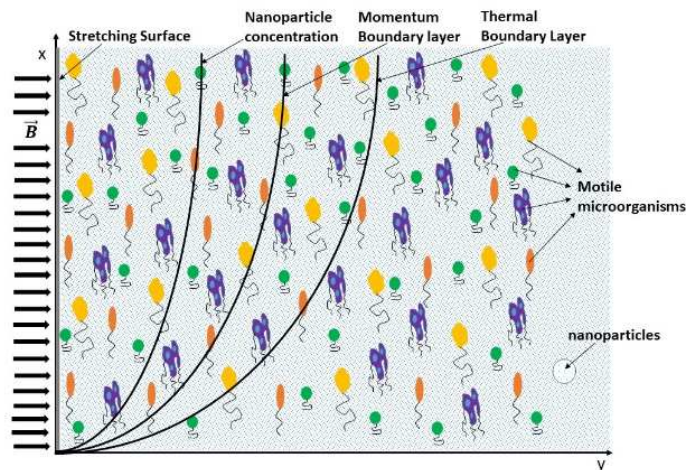

Fig. 1. Schematic diagram the flow field

2. Mathematical Formulation

Casson nanofluid flow with gyrotactic micro-organisms and applied magnetic field on a nonlinear stretching sheet witnessing Joule and viscous dissipation is looked over. Boundary surface stretches with velocity $a\bar{\xi}^p$ (where $a > 0$ and p are constant). Sheet is considered in vertically upward direction (i.e. along $\bar{\xi}$ − axis). The value of unknown functions (i.e. temperature, nanoparticle concentration, and motile micro-organisms density) at the boundary surface is $\bar{\theta}_b$, $\bar{\varphi}_b$ and $\bar{\chi}_b$ respectively, and these are larger than that of free stream i.e. $\bar{\theta}_{fs}$, $\bar{\varphi}_{fs}$ and $\bar{\chi}_{fs}$ respectively. A schematic figure demonstrating the flow field is depicted in figure 1. Following the experimental studies [36, 53-56] and models reported in literature [27, 57-61], the mathematical representation of the flow system is represented in Equations (1) - (5):

$$\frac{\partial f_1}{\partial \bar{\xi}} + \frac{\partial f_2}{\partial \bar{\eta}} = 0 \tag{1}$$

$$\rho_f\left(f_1 \frac{\partial f_1}{\partial \bar{\xi}} + f_2 \frac{\partial f_1}{\partial \bar{\eta}}\right) = \mu\left(1 + \frac{1}{\beta}\right)\frac{\partial^2 f_1}{\partial \bar{\eta}^2} + [(1 - \bar{\varphi}_{fs})\rho_{f_1} g \beta_T (\bar{\theta} - \bar{\theta}_{fs}) - (\rho_p - \rho_{f_1})g(\bar{\varphi} - \bar{\varphi}_{fs}) - g\gamma(\rho_{\bar{\chi}} - \rho_{f_1})(\bar{\chi} - \bar{\chi}_{fs})] - \sigma B^2 f_1 \tag{2}$$

$$f_1 \frac{\partial \bar{\theta}}{\partial \bar{\xi}} + f_2 \frac{\partial \bar{\theta}}{\partial \bar{\eta}} = \alpha \frac{\partial^2 \bar{\theta}}{\partial \bar{\eta}^2} + \tau\left[D_B \frac{\partial \bar{\varphi}}{\partial \bar{\eta}}\frac{\partial \bar{\theta}}{\partial \bar{\eta}} + \frac{D_{\bar{\theta}}}{\bar{\theta}_{fs}}\left(\frac{\partial \bar{\theta}}{\partial \bar{\eta}}\right)^2\right] + \frac{A'''}{(\rho c)_f} + \frac{\sigma B^2}{\rho c_p}f_1^2 + \frac{v}{c_p}\left(1 + \frac{1}{\beta}\right)\left(\frac{\partial f_1}{\partial \bar{\eta}}\right)^2 \tag{3}$$

$$f_1 \frac{\partial \bar{\varphi}}{\partial \bar{\xi}} + f_2 \frac{\partial \bar{\varphi}}{\partial \bar{\eta}} = D_B \frac{\partial^2 \bar{\varphi}}{\partial \bar{\eta}^2} + \frac{D_{\bar{\theta}}}{\bar{\theta}_{fs}}\frac{\partial^2 \bar{\theta}}{\partial \bar{\eta}^2}, \tag{4}$$

$$f_1 \frac{\partial \overline{\chi}}{\partial \overline{\xi}} + f_2 \frac{\partial \overline{\chi}}{\partial \overline{\eta}} = D_{\overline{\chi}} \frac{\partial^2 \overline{\chi}}{\partial \overline{\eta}^2} - \frac{b\omega_c}{\overline{\varphi}_b - \overline{\varphi}_{fs}} \left(\frac{\partial \overline{\chi}}{\partial \overline{\eta}} \frac{\partial \overline{\varphi}}{\partial \overline{\eta}} + \overline{\chi} \frac{\partial^2 \overline{\varphi}}{\partial \overline{\eta}^2} \right),$$ (5)

where, f_1 and f_2 are velocity components along $\overline{\xi}$ and $\overline{\eta}$ directions, respectively. The parameters $D_{\overline{g}}, \gamma, \omega_c$ and b are, respectively, thermophoresis diffusion coefficient, the average volume of a microorganism, maximum cell swimming speed and chemotaxis constant. The meaning of other symbols is the same as defined in [62]. No pressure gradient is applied in flow system and $B = B_0 \overline{\xi}^{(p-1)/2}$ [63].

The associated boundary conditions are

$$at \ \overline{\eta} = 0 : f_1 = a\overline{\xi}^p ; f_2 = 0; \overline{\theta} = \overline{\theta}_b ; D_B \frac{\partial \overline{\varphi}}{\partial \overline{\eta}} + \frac{D_{\overline{g}}}{\overline{\theta}_{fs}} \frac{\partial \overline{\theta}}{\partial \overline{\eta}} = 0; \overline{\chi} = \overline{\chi}_b,$$

$$as \ \overline{\eta} \to \infty : f_1 \to 0; \frac{\partial f_1}{\partial \overline{\eta}} \to 0; \overline{\theta} \to \overline{\theta}_{fs} ; \overline{\varphi} \to \overline{\varphi}_{fs} ; \overline{\chi} \to \overline{\chi}_{fs}.$$ (6)

The non-uniform heat source/sink A''' is modeled as [62]

$$A''' = \left(\frac{ak\overline{\xi}^p}{\overline{\xi}v} \right) [A^*(\overline{\theta}_b - \overline{\theta}_{fs})f' + B^*(\overline{\theta} - \overline{\theta}_{fs})].$$ (7)

in which $A^*, B^* > 0 / A^*, B^* < 0$, signifies an internal heat source/sink. We consider the following dimensionless variables

$$\eta = \left(\frac{\overline{\eta}}{\overline{\xi}} \right) Re_{\overline{\xi}}^{\frac{1}{2}}, \xi = \frac{Gr_{\overline{\xi}}}{Re_{\overline{\xi}}^2}, \psi(\overline{\xi}, \overline{\eta}) = vRe_{\overline{\xi}}^{\frac{1}{2}} f(\eta, \xi), f_1 = \frac{vRe_{\overline{\xi}}}{\overline{\xi}} \frac{\partial f}{\partial \eta} \Bigg|$$

$$f_2 = -\frac{vRe_{\overline{\xi}}^{\frac{1}{2}}}{\overline{\xi}} \left\{ \frac{1+p}{2} f - \frac{1-p}{2} \eta \frac{\partial f}{\partial \eta} + (1-2p)\xi \frac{\partial f}{\partial \xi} \right\},$$ (8)

$$\theta(\eta, \xi) = \frac{\overline{\theta} - \overline{\theta}_{fs}}{\overline{\theta}_b - \overline{\theta}_{fs}}, \varphi(\eta, \xi) = \frac{\overline{\varphi} - \overline{\varphi}_{fs}}{\overline{\varphi}_b - \overline{\varphi}_{fs}}, \chi(\eta, \xi) = \frac{\overline{\chi} - \overline{\chi}_{fs}}{\overline{\chi}_b - \overline{\chi}_{fs}},$$

where, f, θ, φ and χ are stream function satisfying continuity equation, dimensionless temperature, dimensionless nanoparticle concentration, and dimensionless microorganism density. $Gr_{\overline{\xi}} = \{(1 - \overline{\varphi}_{fs})\rho_{f_1} g \beta_T (\overline{\theta}_b - \overline{\theta}_{fs})\}\overline{\xi}^3 / \rho_f v^2$ is the local Grashof number and $Re_{\overline{\xi}} = a\overline{\xi}^{p+1} / v$ is the local Reynolds number. Eqns. (1)-(5), under the transformation (8), take the form

$$\left(1 + \frac{1}{\beta}\right) \frac{\partial^3 f}{\partial \eta^3} + \left(\frac{1+p}{2}\right) f \frac{\partial^2 f}{\partial \eta^2} - p \left(\frac{\partial f}{\partial \eta}\right)^2 - (1-2p)\xi \left(\frac{\partial^2 f}{\partial \xi \partial \eta} \frac{\partial f}{\partial \eta} - \frac{\partial^2 f}{\partial \eta^2} \frac{\partial f}{\partial \xi} \right) + \xi(\theta - Nr\varphi - Rb\chi) - M \frac{\partial f}{\partial \eta} = 0$$ (9)

$$\frac{\partial^2 \theta}{\partial \eta^2} + Pr\left[Nb \frac{\partial \varphi}{\partial \eta} \frac{\partial \theta}{\partial \eta} + Nt \left(\frac{\partial \theta}{\partial \eta}\right)^2 \right] + A^* f' + B^* \theta + \left(\frac{1+p}{2}\right) Prf \frac{\partial \theta}{\partial \eta} - Pr(1-2p)\xi \left(\frac{\partial f}{\partial \eta} \frac{\partial \theta}{\partial \xi} - \frac{\partial \theta}{\partial \eta} \frac{\partial f}{\partial \xi} \right) + PrEc \left[M \left(\frac{\partial f}{\partial \eta}\right)^2 + \left(1 + \frac{1}{\beta}\right) \left(\frac{\partial^2 f}{\partial \eta^2}\right)^2 \right] = 0$$ (10)

$$\frac{\partial^2 \varphi}{\partial \eta^2} + \left(\frac{1+p}{2}\right) Lef \frac{\partial \varphi}{\partial \eta} + \frac{Nt}{Nb} \frac{\partial^2 \theta}{\partial \eta^2} - Le(1-2p)\xi \left(\frac{\partial f}{\partial \eta} \frac{\partial \varphi}{\partial \xi} - \frac{\partial \varphi}{\partial \eta} \frac{\partial f}{\partial \xi} \right) = 0$$ (11)

$$\frac{\partial^2 \chi}{\partial \eta^2} - Pe \left(\frac{\partial \chi}{\partial \eta} \frac{\partial \varphi}{\partial \eta} + (\Omega + \chi) \frac{\partial^2 \varphi}{\partial \eta^2} \right) - Lb(1-2p)\xi \left(\frac{\partial f}{\partial \eta} \frac{\partial \chi}{\partial \xi} - \frac{\partial \chi}{\partial \eta} \frac{\partial f}{\partial \xi} \right) = 0,$$ (12)

and the associated boundary conditions become

$$\frac{\partial f}{\partial \eta}(0, \xi) = 1, f(0, \xi) = 0, \theta(0, \xi) = 1, Nb \frac{\partial \varphi(0, \xi)}{\partial \eta} + Nt \frac{\partial \theta(0, \xi)}{\partial \eta} = 0, \chi(0, \xi) = 1$$

$$\frac{\partial f}{\partial \eta}(\infty, \xi) \to 0, \theta(\infty, \xi) \to 0, \varphi(\infty, \xi) \to 0, \chi(\infty, \xi) \to 0$$ (13)

where, the governing parameters are

$$M = \sigma B_0^2 / a\rho, Pr = v / \alpha, Ec = a^2 \overline{\xi}^{2p} / (c_p(\overline{\theta}_b - \overline{\theta}_{fs})),$$
$$Nb = \tau D_B(\overline{\varphi}_b - \overline{\varphi}_{fs}) / v, Nt = \tau D_{\overline{g}}(\overline{\theta}_b - \overline{\theta}_{fs}) / (v\overline{\theta}_{fs}),$$
$$Nr = (\rho_p - \rho_{f_1})(\overline{\varphi}_b - _{fs}) / \rho_{f_1}\beta_T(\overline{\theta}_b - \overline{\theta}_{fs})(1 - \overline{\varphi}_{fs}),$$
$$Lb = v / D_{\overline{\chi}}, Pe = b\omega_c / D_{\overline{\chi}}, \Omega = \overline{\chi}_{fs} / (\overline{\chi}_b - \overline{\chi}_{fs}),$$
$$Rb = \gamma(\rho_{\overline{\chi}} - \rho_{f_1})(\overline{\chi}_b - \overline{\chi}_{fs}) / \rho_{f_1}\beta_T(\overline{\theta}_b - \overline{\theta}_{fs})(1 - \overline{\varphi}_{fs}),$$
$$Le = v / D_B, \ \alpha = k / \rho c_f,$$

where, Lb, Pe, Ω and Rb are respectively, bio-convective Lewis number, bio-convective Peclet number, Microorganism concentration difference parameter, and bio-convective Rayleigh number. Skin friction coefficient $Sf_{\overline{\xi}}$, heat transfer rate $Ht_{\overline{\xi}}$, nanoparticle transfer rate $Ct_{\overline{\xi}}$ and motile microorganism transfer rate $Mt_{\overline{\xi}}$ at the stretching surface $(i.e. \eta = 0)$ are defined as:

$$Sf_{\overline{\xi}} Re_{\overline{\xi}}^{1/2} = \left(1 + \frac{1}{\beta}\right) \frac{\partial^2 f}{\partial \eta^2}, \quad Ht_{\overline{\xi}} Re_{\overline{\xi}}^{-1/2} = -\frac{\partial \theta}{\partial \eta}, \quad Ct_{\overline{\xi}} Re_{\overline{\xi}}^{-1/2} = -\frac{\partial \overline{\varphi}}{\partial \eta}, \quad Mt_{\overline{\xi}} Re_{\overline{\xi}}^{-1/2} = -\frac{\partial \chi}{\partial \eta}.$$

3. Solution Technique

To get the solution of system (9) - (12) subject to (13), we exercise a numerical algorithm for system of PDEs known as paired quasilinearisation method (PQLM). Detail explanation of the PQLM algorithm is mentioned in Otegbeye et al. [64] and Mumukshu et al. [65]. The PQLM draws on the concept of quasilinearisation that seeks to linearize a system of nonlinear equations by applying the Taylor series expansion before collocating and solving the linearized system. The innovation of the PQLM however, lies in decoupling a large coupled system into pairs of equations so as to reduce the size of matrices that are to be inverted thereby minimizing computational cost. In this regard, we observe that derivatives of θ and φ are coupled in one of the boundary conditions so the PQLM is a suitable method and we will pair θ and while f and χ will be the initial pairing. We begin by applying quasilinearisation on f , χ and their corresponding derivatives in equations (the first and last equations). This gives the pair

$$\left(1+\frac{1}{\beta}\right)f'''_{r+1}+1+[a_1]f''_{r+1}+1+[a_2]f'_{r+1}+1+[a_3]f_{r+1}+(-Rb\xi)\chi_{r+1}=[a_4]\frac{\partial f'_{r+1}}{\partial \xi}+[a_5]\frac{\partial f_{r+1}}{\partial \xi}+a_6$$

$$[b_1]f'_{r+1}+\chi''_{r+1}+[b_2]\chi'_{r+1}+[b_3]\chi_{r+1}=[b_4]\frac{\partial f_{r+1}}{\partial \xi}+[b_5]\frac{\partial \chi_{r+1}}{\partial \xi}+b_6$$

(14)

where

$$\alpha_1=\frac{1+p}{2}, \ \alpha_2=1-2p, \ a_1=\alpha_1 f_r+\alpha_2\xi\frac{\partial f_r}{\partial \xi}, \ a_2=-2pf'_r-\alpha_2\xi\frac{\partial f'_r}{\partial \xi},$$

$$a_3=\alpha_1 f''_r, \ a_4=\alpha_2\xi f'_r, \ a_5=-\alpha_2\xi f''_r,$$

$$a_6=\alpha_1 f_r f''_r-pf'^2_r-\alpha_2\xi(f'_r\frac{\partial f'_r}{\partial \xi}-f''_r\frac{\partial f_r}{\partial \xi})-\xi(\theta_r-Nr\varphi_r),$$

$$b_1=-Lb\alpha_2\xi\frac{\partial \chi_{r+1}}{\partial \xi}, \ \ b_2=-Pe\varphi'_r+Lb\alpha_2\xi\frac{\partial f_r}{\partial \xi},$$

$$b_3=-Pe\varphi''_r, \ \ b_4=-Lb\alpha_2\xi\chi'_{r+1}, \ \ b_5=Lb\alpha_2\xi f'_r,$$

$$b_6=Pe\omega\varphi''_r-Lb\alpha_2\xi f'_r\frac{\partial \chi_{r+1}}{\partial \xi}+Lb\alpha_2\xi\chi'_{r+1}\frac{\partial f_r}{\partial \xi}.$$

Current solutions for f , χ are used in the second pair of equations (i.e (10) and (11)). Linearising θ and φ as above yield the pair

$$\theta''_{r+1}+[c_1]\theta'_{r+1}+B^*\theta_{r+1}+[c_2]\varphi'_{r+1}=[c_3]\frac{\partial \theta_{r+1}}{\partial \xi}+c_4,$$

$$\frac{Nt}{Nb}\theta''_{r+1}+\varphi''_{r+1}+[e_1]\varphi'_{r+1}=[e_2]\frac{\partial \varphi_{r+1}}{\partial \xi},$$

(15)

where

$$c_1=PrNb\varphi'_r+2PrNt\theta'_r+\alpha_1 Prf_{r+1}+Pr\alpha_2\xi\frac{\partial f_{r+1}}{\partial \xi},$$

$$c_2=PrNb\theta'_r, \ \ c_3=Pr\alpha_2\xi f'_{r+1},$$

$$c_4=PrNb\theta'_r\varphi'_r+PrNt\theta'^2_r-A^*\exp^{-\eta}-PrMEcf'^2_r-\left(1+\frac{1}{\beta}\right)PrEcf''^2_{r+1},$$

$$e_1=\alpha_1 Lef_{r+1}+Le\alpha_2\xi\frac{\partial f_{r+1}}{\partial \xi}, \ \ e_2=Le\alpha_2\xi f'_{r+1}.$$

The linearized pairs (14) and (15) are solved using the Chebyshev spectral method. To achieve this we transform the pairs from domains $\eta\in[0,\eta_\infty]$ and $\xi\in[0,\xi_\infty]$ to $x,y\in[-1,1]$, respectively, where η_∞ and ξ_∞ are fixed constants. We assume the approximate solutions are defined using bivariate Lagrange interpolation polynomials of the form

$$E(\eta,\xi)\approx\sum_{i=0}^{M_x}\sum_{j=0}^{M_y}E\left(x_i,y_j\right)L_m(x)L_j(y), \qquad E=f,\chi,\theta,\varphi$$

(16)

which interpolates $E(\eta,\xi)$ at x_i and y_j where

$$x_i=\cos\left(\frac{\pi i}{M_x}\right), \ y_j=\cos\left(\frac{\pi j}{M_y}\right), \ i=0,1,\ldots,M_x, \ j=0,1,\ldots,M_y$$

are Gauss-Lobatto collocation points. The derivatives of unknown functions from pairs (14) and (15) are represented using the Chebyshev spectral method in the form

$$\frac{\partial^m E}{\partial \eta^m}\bigg|_{(x_k,y_i)}=\mathbf{D}^m\mathbf{E}_i, \ m=1,2,3$$

$$\frac{\partial E}{\partial \xi}\bigg|_{(x_k,y_i)}=\sum_{j=0}^{M_y}\mathbf{d}_{ij}\mathbf{F}_j,$$

(17)

where $\mathbf{D} = 2D_{l,k} / \eta_\infty$, $l,k = 0,...,M_x$, with $D_{l,k}$ being a differentiation matrix with dimension $(M_x + 1) \times (M_x + 1)$. Also, $\mathbf{d} = 2d_{h,q} / \xi_{fs}$, $h,q = 0,...,M_y$ with $d_{l,k}$ being a differentiation matrix with dimension $(M_y + 1) \times (M_y + 1)$ and $\mathbf{E}_i$ being a vector defined thus

$$\mathbf{E}_i = \left[E_i(x_0), E_i(x_1),...,E_i(x_{M_x}) \right]^T . \tag{18}$$

Applying spectral methods on our linearized pairs (14) and (15), we obtain

$$\mathbf{A}_{11,i}\mathbf{F}_{r+1,i} + \mathbf{A}_{12,i}\mathbf{X}_{r+1,i} - [\mathbf{a}_{4,i}]\sum_{j=0}^{M_y}\mathbf{d}_{i,j}\mathbf{DF}_{r+1,j} - [\mathbf{a}_{5,i}]\sum_{j=0}^{M_y}\mathbf{d}_{i,j}\mathbf{F}_{r+1,j} = \mathbf{R}_{1,i},$$

$$\mathbf{A}_{21,i}\mathbf{F}_{r+1,i} + \mathbf{A}_{22,i}\mathbf{X}_{r+1,i} - [\mathbf{b}_{4,i}]\sum_{j=0}^{M_y}\mathbf{d}_{i,j}\mathbf{F}_{r+1,j} - [\mathbf{b}_{5,i}]\sum_{j=0}^{M_y}\mathbf{d}_{i,j}\mathbf{X}_{r+1,j} = \mathbf{R}_{2,i}, \tag{19}$$

and

$$\mathbf{B}_{11,i}\Theta_{r+1,i} + \mathbf{B}_{12,i}\Phi_{r+1,i} - [\mathbf{c}_{5,i}]\sum_{j=0}^{M_y}\mathbf{d}_{i,j}\Theta_{r+1,j} = \mathbf{R}_{3,i},$$

$$\mathbf{B}_{21,i}\Theta_{r+1,i} + \mathbf{B}_{22,i}\Phi_{r+1,i} - [\mathbf{e}_{2,i}]\sum_{j=0}^{M_y}\mathbf{d}_{i,j}\Phi_{r+1,j} = \mathbf{R}_{4,i}, \tag{20}$$

where

$$\mathbf{A}_{11,i} = \left(1 + \frac{1}{\beta}\right)\mathbf{D}^3 + [\mathbf{a}_{1,i}]\mathbf{D}^2 + [\mathbf{a}_{2,i}]\mathbf{D} + [\mathbf{a}_{3,i}], \mathbf{A}_{12,i} = (-Rb\xi)\mathbf{I},$$

$$\mathbf{A}_{21,i} = [\mathbf{b}_{1,i}]\mathbf{D}, \ \mathbf{A}_{22,i} = \mathbf{D}^2 + [\mathbf{b}_{2,i}]\mathbf{D} + [\mathbf{b}_{3,i}] \tag{21}$$

and

$$\mathbf{B}_{11,i} = \mathbf{D}^2 + [\mathbf{c}_{1,i}]\mathbf{D} + (B^*)\mathbf{I}, \ \mathbf{B}_{12,i} = [\mathbf{c}_{2,i}]\mathbf{D},$$

$$\mathbf{B}_{21,i} = \left(\frac{Nt}{Nb}\right)\mathbf{D}^2, \ \mathbf{B}_{22,i} = \mathbf{D}^2 + [\mathbf{e}_1]\mathbf{D}, \tag{22}$$

where $\mathbf{I}$ is an identity matrix of size $(M_x + 1) \times (M_x + 1)$.

Fig. 2. Error of f .
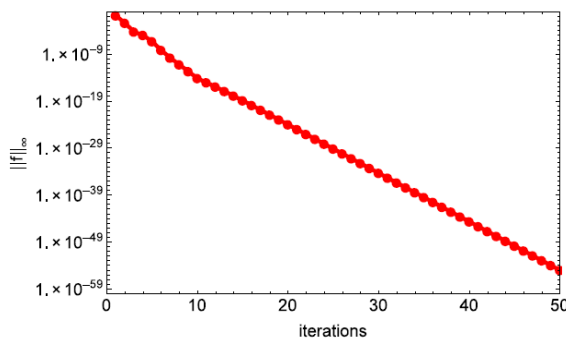

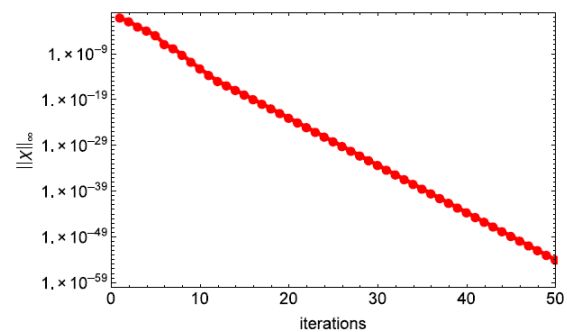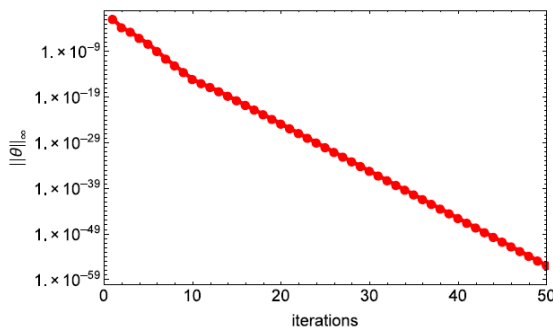**Fig. 3.** Error of χ .

Fig. 4. Error of θ .
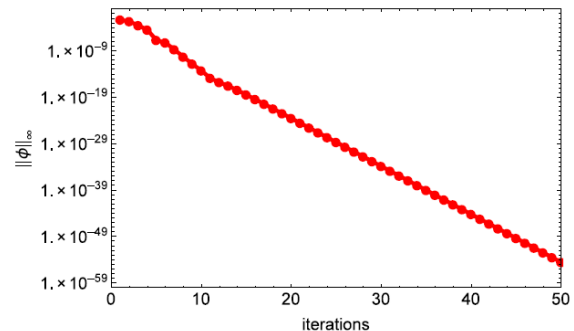
Fig. 5. Error of φ .
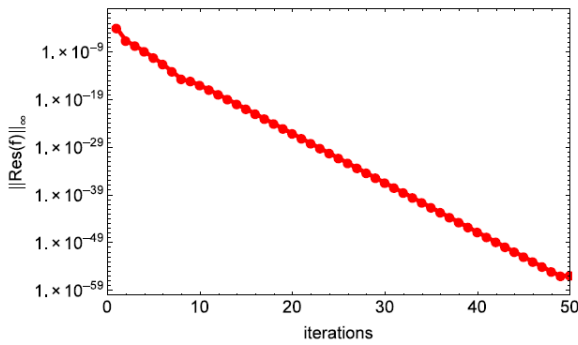
Fig. 6. Residual of f .
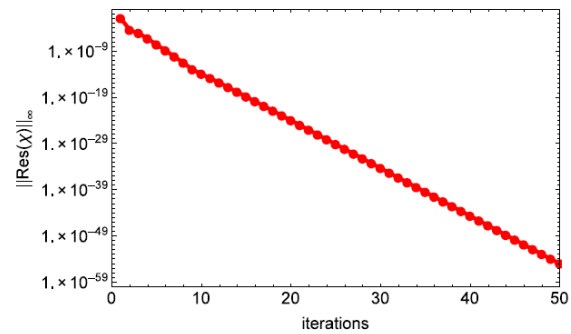
Fig. 7. Residual of χ .
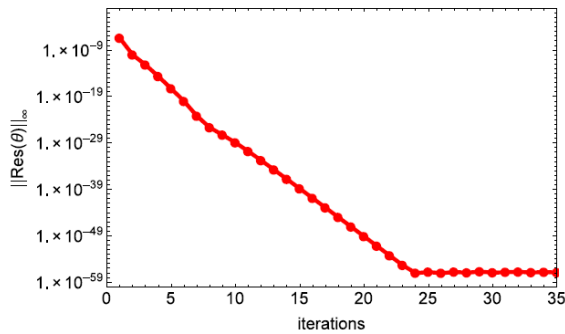
Fig. 8. Residual of θ .
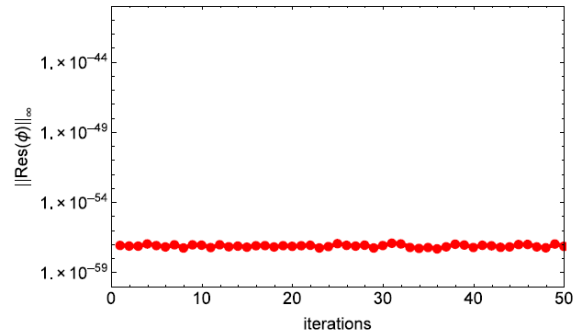
Fig. 9. Residual of φ .

4. Convergence and Accuracy

The system of partial differential equations (9)-(12) along with the boundary condition (13) are solved using the numerical technique, PQLM, described in the previous section and the obtained results are presented graphically. The iteration scheme is set for 80 grid points in space and 10 grid points in time as these were found to be adequate to generate the accurate consistent results. Figures 1-8 are plotted to describe the accuracy and convergence of the obtained solutions by generating solution based error and residual-based error for each, stream function f , species function for the concentration of motile-microorganisms χ , dimensionless temperature θ and nanoparticle concentration function φ .

4.1 Solution error norms

The error between two successive iterations are calculated by keeping $\chi = 0.5$, $M = 2$, $\beta = 0.3$, $p = 0.3$, $Pr = 5$, $Nr = 0.1$, $Nb = 0.1$, $Nt = 0.1$, $A^* = 0.5$, $B^* = 0.5$, $Ec = 0.1$, $Le = 5$, $Pe = 1$, $Lb = 3$, $\Omega = 0.1$ and $Rb = 0.2$ values of flow parameters. The norm of this error is termed as a solution-based error norm. Figures (2)-(5) demonstrate the solution error norms for f, χ, θ and φ , respectively. Here it can be observed that the absolute values of error reduce to a tolerance value of 10^{-54} in 50 iterations. Henceforth, this establishes an excellent convergence of the iteration scheme.

4.2 Residual errors

Figures (6)-(9) shows the residual norms of the solutions of f, χ, θ and φ , respectively. The residual error of the system of PDEs (9) - (12) are evaluated by taking $\chi = 0.5$, $M = 2$, $\beta = 0.3$, $p = 0.3$, $Pr = 5$, $Nr = 0.1$, $Nb = 0.1$, $Nt = 0.1$, $A^* = 0.5$, $B^* = 0.5$, $Ec = 0.1$, $Le = 5$, $Pe = 1$, $Lb = 3$, $\Omega = 0.1$ and $Rb = 0.2$. The residual error is obtained by taking the norm of the values derived by substituting the approximate solution yielded by proposed numerical scheme into the original system (9) - (12). The contiguous proximity of obtained numerical solutions to the analytical solution of the system is delineated by residual error. Here, observe that accuracy of almost 10^{-57} is obtained in 50 iterations in case of f and χ . Moreover, observe that linear progress in the convergence of absolute residual errors f , χ , θ is achieved, as seen in figures (5), (6) and (7) whereas a consistent absolute residual error φ is obtained from the very first iteration, see figure (8). Additionally, note that in figure (7), it takes 24 iterations to achieve the convergence, while 50 iterations are needed in the rest of the cases.

5. Results and Discussion

Numerical results of governing differential equations obtained by implementing PQLM are prepared in graphical and tabular form. A brief discussion on physics related to the influence of relevant flow parameters on dimensionless velocity $f'(\eta, \xi)$, gyrotactic microorganism concentration $\chi(\eta, \xi)$, temperature $\theta(\eta, \xi)$, and nanoparticle concentration $\varphi(\eta, \xi)$ is outlined to examine heat and flow behavior.

5.1 Influence of M on χ

Figure 10 reveals the behavior of motile micro-organism concentration under the effect of the magnetic field. Magnetotactic bacteria (Motile micro-organism), behaves as a self-propelled dipole under influence of magnetic field and it moves along the field

lines. Additionally, the presence of more number of nanoparticles within the boundary layer region creates an upsurge in the inclusive mass density of both nanoparticles and motile microorganisms. Self-gyrating microorganisms tend to move from higher concentration towards the lower concentration, resulting in depletion of concentration of motile microorganisms. Thus, a decrement in motile microorganism concentration in the boundary layer region is observed with an increase in the magnetic parameter (Figure 10).

5.2 Profiles of χ

From figure 11, it is seen that motile micro-organism density increases with the thermophoresis parameter Nt. A peak in motile micro-organism density near the boundary is observed and this peak is more pronounced for a higher value of the thermophoretic parameter. After attaining the peak it decreases steadily to confirm free-stream condition. A rise in thermophoresis creates a larger thermal gradient, this causes the particles to travel from the boundary layer region to the free stream. Similar observations were conveyed in [61].
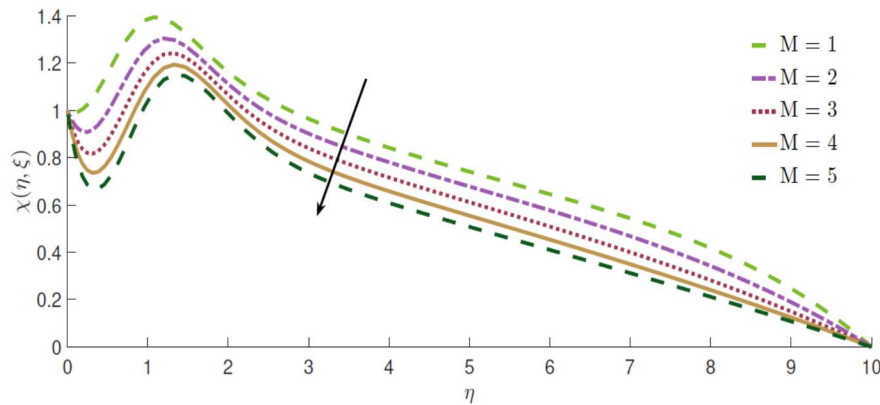

Fig. 10. Effect of M on χ with $\xi = 0.7$, $\beta = 0.1$, $Nr = 0.1$, $p = 0.3$, $Nt = 0.1$, $Rb = 0.2$, $Pr = 5$, $Nb = 0.1$, $A^* = 0.5$, $B^* = 0.5$, $Ec = 0.1$, $Le = 3$, $Pe = 1$, $\Omega = 0.1$ and $Lb = 3$.
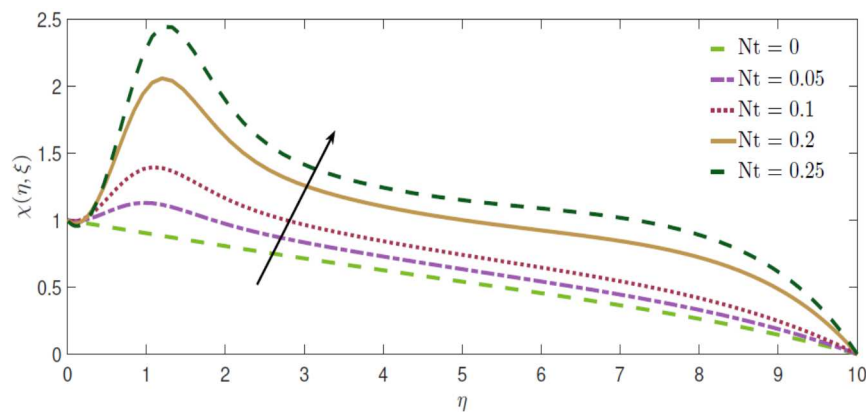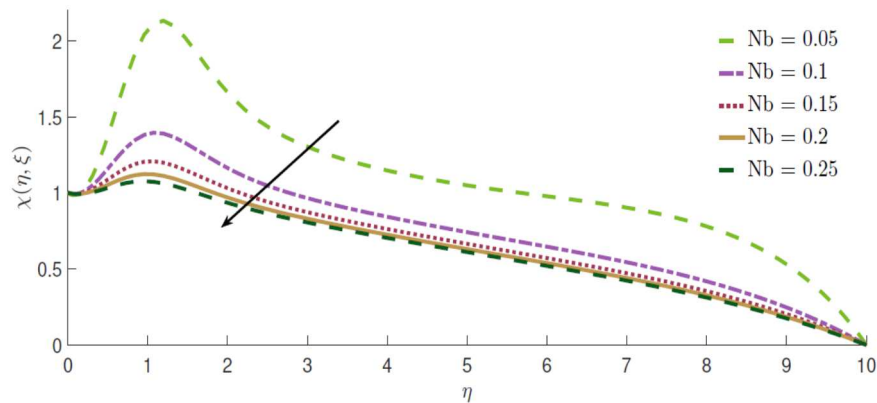

Fig. 11. Profiles of χ with Nt when $\xi = 0.7$, $\beta = 0.1$, $Nr = 0.1$, $p = 0.3$, $M = 1$, $Rb = 0.2$, $Pr = 5$, $Nb = 0.1$, $A^* = 0.5$, $B^* = 0.5$, $Ec = 0.1$, $Le = 3$, $Pe = 1$, $\Omega = 0.1$ and $Lb = 3$.
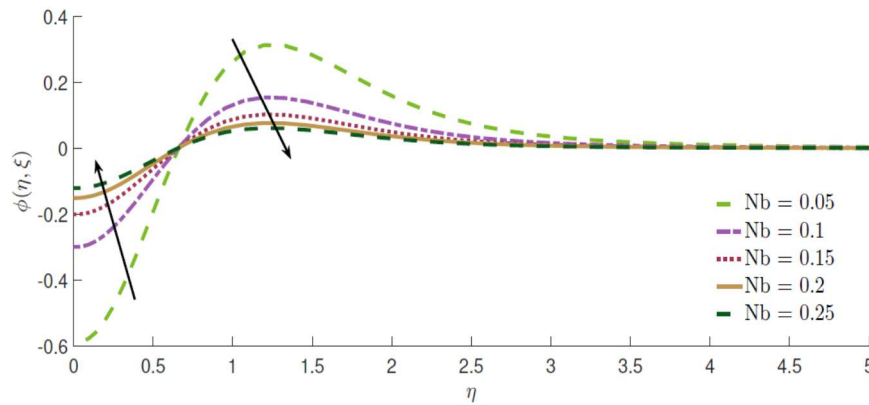

Fig. 12. Effect of Nb on χ when $\xi = 0.7$, $\beta = 0.1$, $Nr = 0.1$, $p = 0.3$, $M = 1$, $Rb = 0.2$, $Pr = 5$, $Nt = 0.1$, $A^* = 0.5$, $B^* = 0.5$, $Ec = 0.1$, $Le = 3$, $Pe = 1$, $\Omega = 0.1$ and $Lb = 3$.

Fig. 13. Effect of Nb on φ when $\xi = 0.7$, $\beta = 0.1$, $Nr = 0.1$, $p = 0.3$, $M = 1$, $Rb = 0.2$, $Pr = 5$, $Nt = 0.1$, $A^* = 0.5$, $B^* = 0.5$, $Ec = 0.1$, $Le = 3$, $Pe = 1$, $\Omega = 0.1$ and $Lb = 3$.
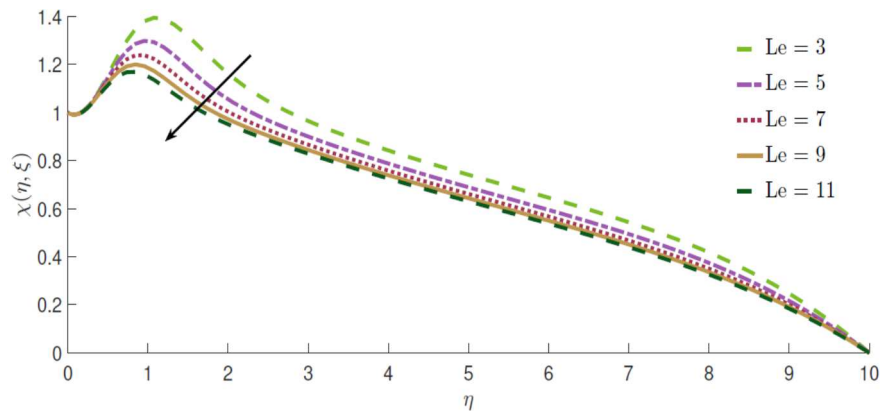

Fig. 14. Effects of Le on χ when $\xi = 0.7$, $\beta = 0.1$, $Nr = 0.1$, $p = 0.3$, $M = 1$, $Rb = 0.2$, $Pr = 5$, $Nt = 0.1$, $A^* = 0.5$, $B^* = 0.5$, $Ec = 0.1$, $Nb = 0.1$, $Pe = 1$, $\Omega = 0.1$ and $Lb = 3$.

Fig. 15. Effects of Le on φ when $\xi = 0.7$, $\beta = 0.1$, $Nr = 0.1$, $p = 0.3$, $M = 1$, $Rb = 0.2$, $Pr = 5$, $Nt = 0.1$, $A^* = 0.5$, $B^* = 0.5$, $Ec = 0.1$, $Nb = 0.1$, $Pe = 1$, $\Omega = 0.1$ and $Lb = 3$.
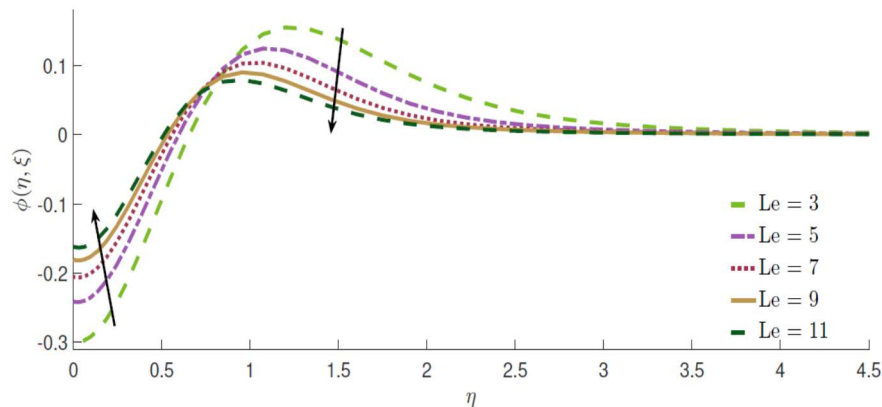
5.3 Effect of Nb on χ and φ

Figures 12 and 13 highlight the nature of concentration profiles of motile micro-organisms and nanoparticle for different values of Brownian motion parameter. Brownian motion is the random movement of a particle in the fluid and it plays a vital role in the multiphase fluid. Brownian motion declines density of microorganisms and nanoparticle concentration. It is interesting to note that, Brownian motion parameter demonstrates a reverse effect on motile microorganisms and nanoparticle concentrations compared to the thermophoresis parameter. Present observation is in good agreement with results in [61, 66].

5.4 Effect of Le on χ and φ

Lewis number is inversely related to the mass diffusion. An elevation in Lewis number results in a reduction in mass diffusion causing a fall in the Brownian diffusion coefficient. Figures 14 and 15 affirm the decrease in motile micro-organisms and nanoparticle concentration, respectively, with an increase in Lewis number.
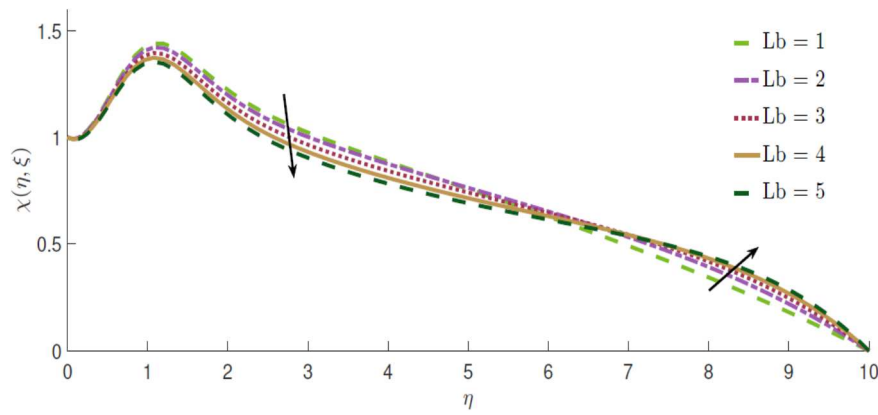
Fig. 16. Effect of bio-convective Lewis number on microorganism density when $\xi = 0.7$, $\beta = 0.1$, $Nr = 0.1$, $p = 0.3$, $M = 1$, $Rb = 0.2$, $Pr = 5$, $Nb = 0.1$, $Nt = 0.1$, $A^* = 0.5$, $B^* = 0.5$, $Ec = 0.1$, $Le = 3$, $Pe = 1$, $\Omega = 0.1$ and $Lb = 3$.
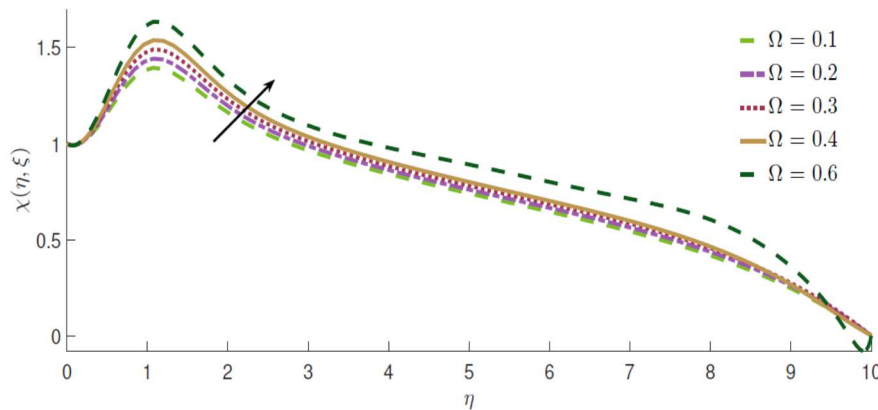

Fig. 17. Effect of Ω on χ profiles when $\xi = 0.7$, $\beta = 0.1$, $Nr = 0.1$, $p = 0.3$, $M = 1$, $Rb = 0.2$, $Pr = 5$, $Nt = 0.1$, $A^* = 0.5$, $B^* = 0.5$, $Ec = 0.1$, $Le = 3$, $Pe = 1$, $Nb = 0.1$ and $Lb = 3$.

Fig. 18. Effect of Buoyancy parameter ξ on χ when $\Omega = 0.1$, $\beta = 0.1$, $Nr = 0.1$, $p = 0.3$, $M = 1$, $Rb = 0.2$, $Pr = 5$, $Nt = 0.1$, $A^* = 0.5$, $B^* = 0.5$, $Ec = 0.1$, $Le = 3$, $Pe = 1$, $\Omega = 0.1$ and $Lb = 3$.
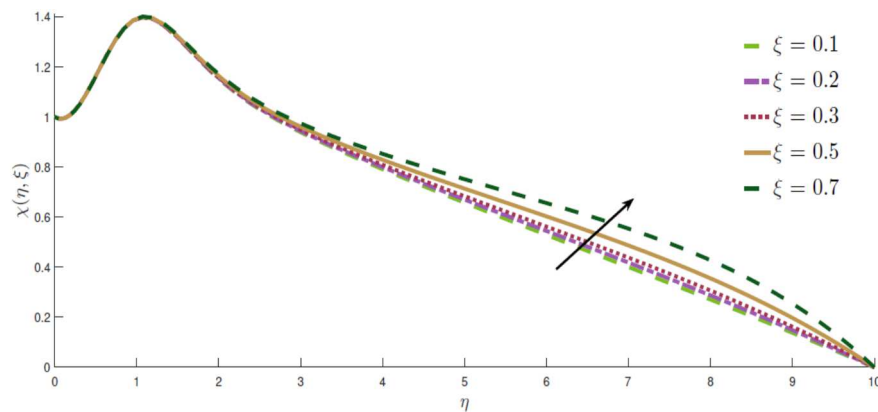
5.5 Effect of Lb on χ

Thermal diffusivity to motile micro-organism mass diffusivity is termed as bio-convection Lewis number, Lb . This parameter characterizes heat transfer due to microbes (in the field of medicine or biology). Decay in motile micro-organism density with bio-convection Lewis number appears and this characteristic is reversed near a free stream (Figure 16). The self-propelled nature of microorganisms causes a change in the profile as there is less bio-convection away from the surface.

5.6 Effect of Ω on χ profiles

Figure 17 exhibits the impact of motile micro-organism concentration difference on microorganism density profiles. The motile micro-organism concentration difference is directly proportional to the free stream concentration and inversely proportional to the difference between concentration at the wall and that in the free stream. Thus, an increase in motile micro-organism concentration difference causes an increase in free stream concentration of micro-organisms. The density of microorganisms develops with Ω as revealed from figure 17.
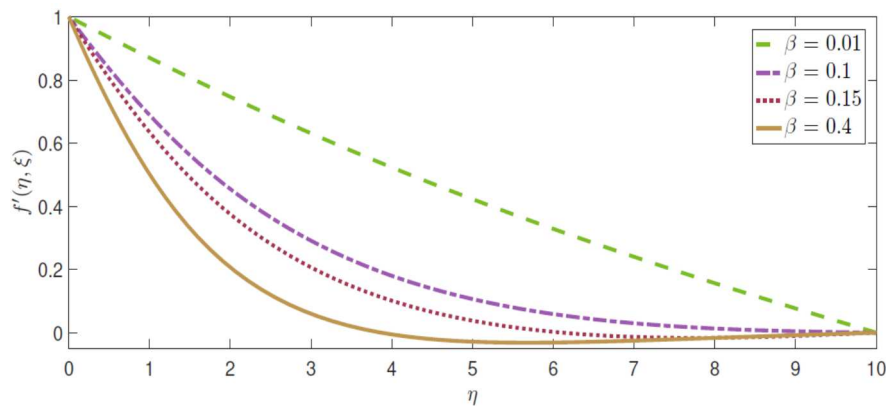
Fig. 19. Effect of Casson parameter β on f' when $\xi = 0.7$, $Nb = 0.1$, $Nr = 0.1$, $p = 0.3$, $M = 1$, $Rb = 0.2$, $Pr = 5$, $Nt = 0.1$, $A^* = 0.5$, $B^* = 0.5$, $Ec = 0.1$, $Le = 3$, $Pe = 1$, $\Omega = 0.1$ and $Lb = 3$.

Fig. 20. Effect of Casson parameter β on θ when $\xi = 0.7$, $Nb = 0.1$, $Nr = 0.1$, $p = 0.3$, $M = 1$, $Rb = 0.2$, $Pr = 5$, $Nt = 0.1$, $A^* = 0.5$, $B^* = 0.5$, $Ec = 0.1$, $Le = 3$, $Pe = 1$, $\Omega = 0.1$ and $Lb = 3$.

Fig. 21. Effect of Casson parameter β on χ when $\xi = 0.7$, $Nb = 0.1$, $Nr = 0.1$, $p = 0.3$, $M = 1$, $Rb = 0.2$, $Pr = 5$, $Nt = 0.1$, $A^* = 0.5$, $B^* = 0.5$, $Ec = 0.1$, $Le = 3$, $Pe = 1$, $\Omega = 0.1$ and $Lb = 3$.
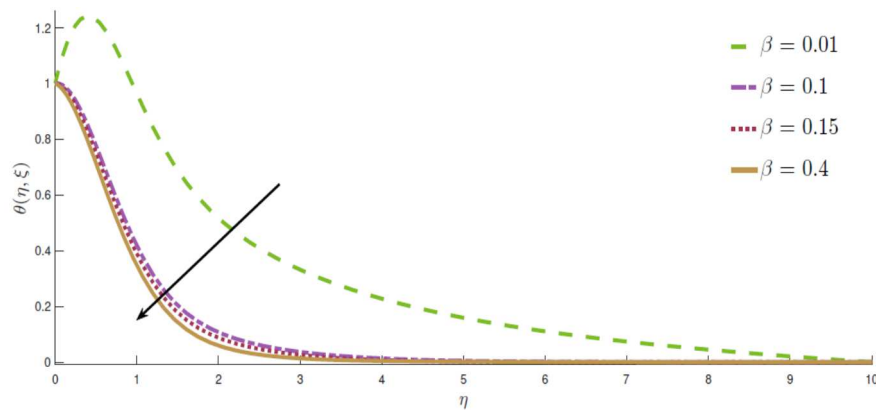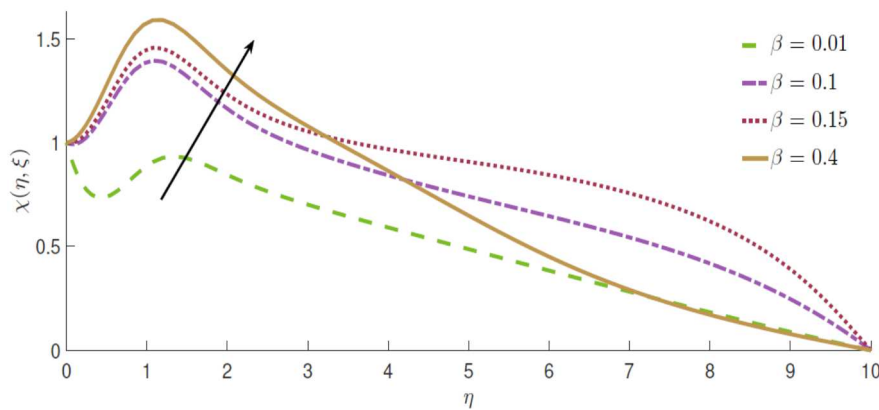
5.7 Effect of Buoyancy parameter ξ on χ

The effect of the buoyancy parameter on microorganism density profiles is shown in figure 18. Motile micro-organism concentration augments with an increase in the buoyancy parameter. Due to bio-convection and self-gyration of microorganisms near the surface, the augmentation by means of buoyancy parameter is more notable away from the surface.

5.8 Effect of Casson parameter β on f', θ, χ and φ

Figures 19-22 illustrate the action of variation in the Casson parameter on velocity, temperature, mobile micro-organism concentration, and nanoparticle concentration profiles, respectively. Larger values of the Casson parameter develop a stronger resistance to the yield stresses, this reduces the velocity of fluid flow. Figures 19 and 20 show that the Casson parameter causes a decline in velocity and temperature profiles. For very small values (i.e. here $\beta = 0.01$) velocity profile is almost linear and a boost in temperature at the vicinity of sheet is observed whereas figures 21 and 22 demonstrate growth in motile micro-organism concentration and nanoparticle concentration profiles with increment in Casson parameter.
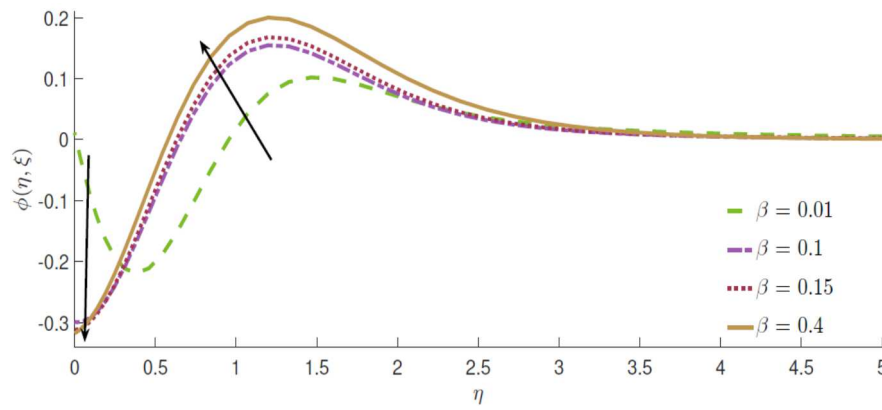
Fig. 22. Effect of Casson parameter β on φ when $\xi = 0.7$, $Nb = 0.1$, $Nr = 0.1$, $p = 0.3$, $M = 1$, $Rb = 0.2$, $Pr = 5$, $Nt = 0.1$, $A^* = 0.5$, $B^* = 0.5$, $Ec = 0.1$, $Le = 3$, $Pe = 1$, $\Omega = 0.1$ and $Lb = 3$.

Fig. 23. Effect of Eckert number Ec on χ when $\xi = 0.7$, $Nb = 0.1$, $Nr = 0.1$, $p = 0.3$, $M = 1$, $Rb = 0.2$, $Pr = 5$, $Nt = 0.1$, $A^* = 0.5$, $B^* = 0.5$, $\beta = 0.1$, $Le = 3$, $Pe = 1$, $\Omega = 0.1$ and $Lb = 3$.

Fig. 24. Effect of Eckert number Ec on θ when $\xi = 0.7$, $Nb = 0.1$, $Nr = 0.1$, $p = 0.3$, $M = 1$, $Rb = 0.2$, $Pr = 5$, $Nt = 0.1$, $A^* = 0.5$, $B^* = 0.5$, $\beta = 0.1$, $Le = 3$, $Pe = 1$, $\Omega = 0.1$ and $Lb = 3$.
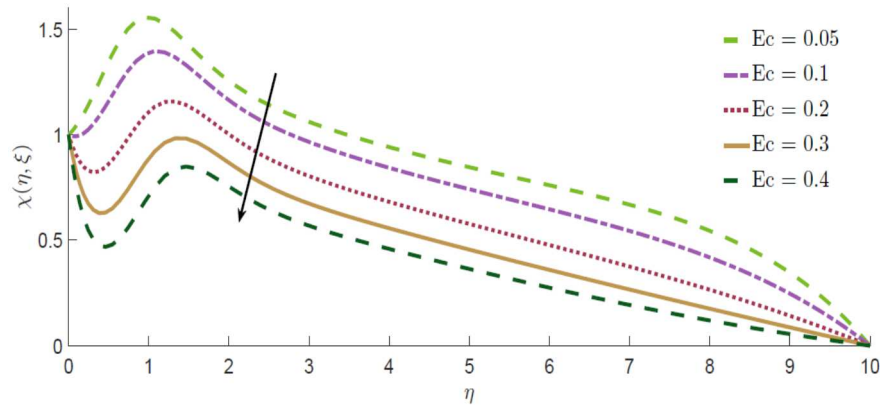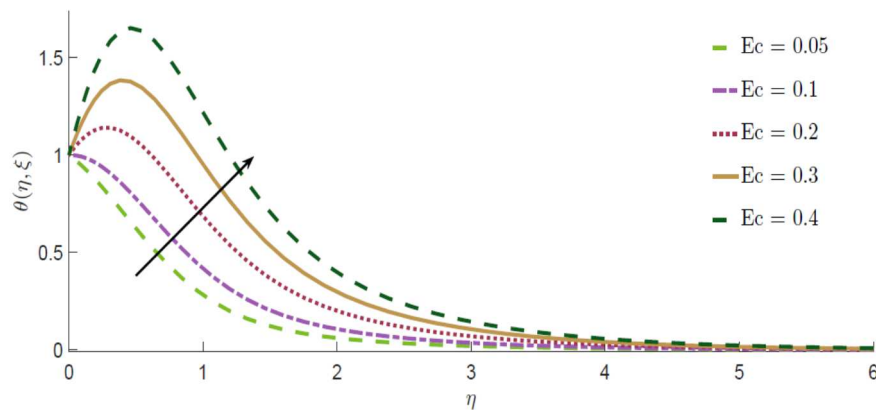
5.9 Effect of Eckert number Ec on θ and χ

Figures 23 and 24 present the behavior of microorganisms concentration and temperature with Eckert number Ec. Figure 23 shows a drop in microorganism concentration with growth in the Eckert number. In fact, advective mass transport proliferates with an increase in Eckert number. This sequentially alters the microorganism concentration in the boundary layer region. Note that, an increase in Eckert number retards the heat dissipation causing the fluid in the boundary region to store more heat, crafting an elevation in the fluid temperature. This is clearly depicted in figure 24.

5.10 Effect of Peclet number Pe on χ

Alteration of microorganism concentration due to Peclet number Pe is viewed in figure 25. It is very clear that the Peclet number boosts the concentration of motile microorganisms in the boundary layer region. More microorganisms gather near the boundary for higher Pe. The phenomenon of an increase in the rate of transport due to advection and a decrease in the rate of mass diffusion occurs with an elevation in Peclet number. This result agrees with the results conveyed by [58] and [61]. This significantly validates the mathematical model and numerical results obtained by PQLM.
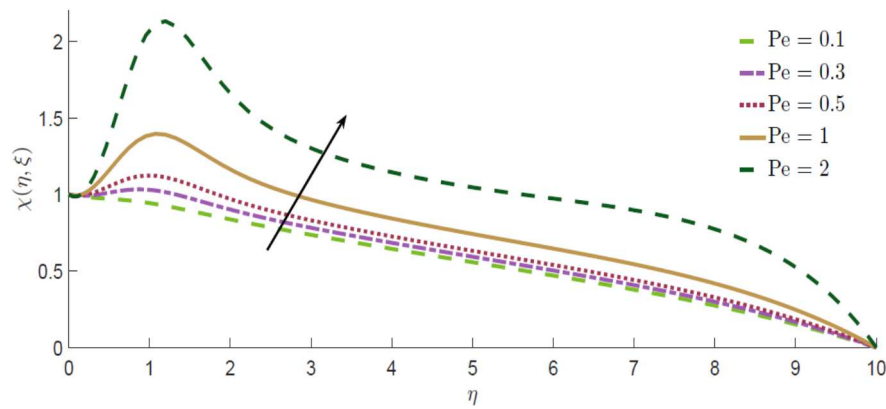
Fig. 25. Effect of Peclet number Pe on χ when $\xi = 0.7$, $Nb = 0.1$, $Nr = 0.1$, $p = 0.3$, $M = 1$, $Rb = 0.2$, $Pr = 5$, $Nt = 0.1$, $A^* = 0.5$, $B^* = 0.5$, $\beta = 0.1$, $Le = 3$, $Ec = 0.1$, $\Omega = 0.1$ and $Lb = 3$.
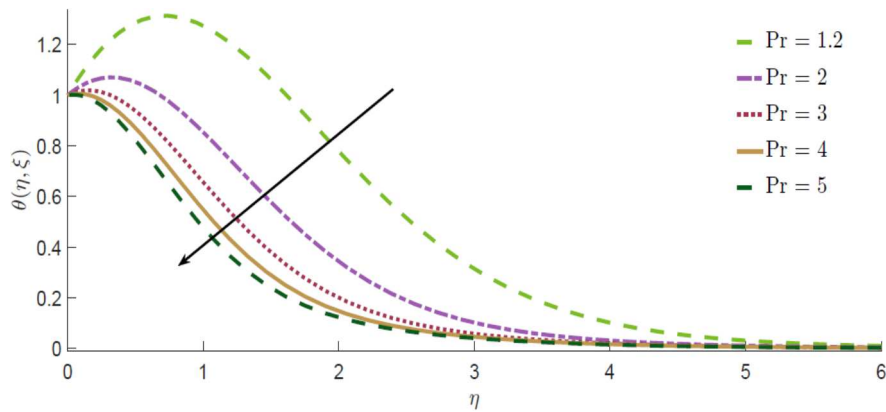

Fig. 26. Effect of Prandtl number Pr on θ when $\xi = 0.7$, $Nb = 0.1$, $Nr = 0.1$, $p = 0.3$, $M = 1$, $Rb = 0.2$, $Ec = 0.1$, $Nt = 0.1$, $A^* = 0.5$, $B^* = 0.5$, $\beta = 0.1$, $Le = 3$, $Pe = 1$, $\Omega = 0.1$ and

Fig. 27. Effect of Prandtl number Pr on χ when $\xi = 0.7$, $Nb = 0.1$, $Nr = 0.1$, $p = 0.3$, $M = 1$, $Rb = 0.2$, $Ec = 0.1$, $Nt = 0.1$, $A^* = 0.5$, $B^* = 0.5$, $\beta = 0.1$, $Le = 3$, $Pe = 1$, $\Omega = 0.1$ and $Lb = 3$
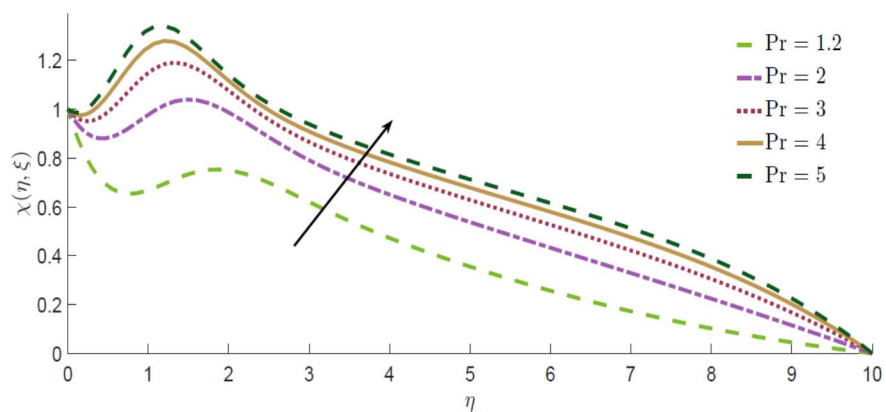
5.11 Effect of Prandtl number Pr on θ and χ

The tendency of temperature and motile microorganism concentration with Prandtl number is examined through graphs 26 and 27. Prandtl number exerts enhancing and declining influence on microorganism concentration and temperature profiles, respectively, throughout the boundary layer region. A distinguished peak is observed in both the profiles at approximately $(\eta \approx 1)$. This is in accordance with the analysis given by [60].

Table 1 exhibits the values of drag coefficient, rate of heat transfer and density of motile micro-organism at the sheet with Prandtl number, Eckert number, Peclet number, and bio convective Lewis number. The ascending value of the Prandtl number implies a weakening of thermal diffusivity. This deteriorated thermal diffusivity produces a drop in heat transfer and density of motile micro-organism and a gain in friction at the surface. Eckert number and Peclet number have enhancing influence in heat transfer and density of motile micro-organism whereas skin friction decreases with Eckert number and Lb increases with Peclet number. The density of motile micro-organism grows and heat transfer declines to a slight extent at sheet with Lb.

Table 1. Effect of some parameters on the skin friction, Nusselt number, and micro-organism density number

Pr	Ec	Pe	Lb	$\left(1+\dfrac{1}{\beta}\right)f''(0,\xi)$	$-\theta'(0,\xi)$	$-\chi'(0,\xi)$
1.2	0.1	1	3	-2.485682	-0.837768	1.096887
2				-3.123754	-0.425208	0.633105
4				-3.525056	-0.143228	0.336019
5				-3.607842	-0.082982	0.274772
	0.05			- 3.305515	-0.182080	0.373070
	0.1			-3.123754	-0.425208	0.633105
	0.2			- 2.775484	-0.887255	1.130341
	0.3			-2.441659	-1.325233	1.603242
		0.5		-3.110248	-0.422251	0.381327
		1		-3.123754	-0.425208	0.633105
		1.5		-3.138434	-0.428344	0.888283
		2		-3.154388	-0.431658	1.147240
			1	-3.131223	-0.426688	0.620892
			2	-3.127421	-0.425939	0.626977
			3	-3.123754	-0.425208	0.633105
			4	-3.120567	-0.424573	0.638639

6. Conclusion

Effects of irregular heat source/sink, Joule and viscous dissipations, Brownian motion, thermophoresis, gyrotactic microorganism and nanoparticles in the bio-convection magnetohydrodynamic flow of Casson fluid was studied at the nonlinear stretching boundary. The non-dimensionalised model outlining the flow system was worked out by pairing, i.e. first pair momentum and gyrotactic micro-organism density equation and second pair energy and nanoparticle concentration equation. This technique was termed as a paired quasilinearisation method (PQLM). Convergence and accuracy of PQLM were shown. Obtained numerical results were presented in graphs and tables. A sharp increase in microorganism concentration which attains the highest level near the stretching boundary was observed after this it declined gradually to reach free stream value. Thermophoresis and Brownian motion show opposite behavior on microorganism concentration i.e. thermophoresis exert increasing whereas Brownian motion decreasing influence. The density of motile microorganisms at the sheet grows with a bio-convective Lewis number. Peclet number gives rise to the density of motile microorganism.

Acknowledgments

Conflict of Interest

The authors declared no potential conflicts of interest with respect to the research, authorship and publication of this article.

Funding

Nomenclature

f_1	velocity components along $\bar{\xi}$ directions	Rb	bio-convective Rayleigh number
f_2	velocity components along $\bar{\eta}$ directions	M	magnetic parameter
f	stream function	Nb	Brownian motion parameter
$\bar{\theta}$	Temperature function	Le	Lewis number
$\bar{\varphi}$	nanoparticle concentration function	Pr	Prandtl number
$\bar{\chi}$	microorganism density function	Nt	thermophoresis parameter
θ	dimensionless temperature	Nr	Buoyancy ratio parameter
φ	dimensionless nanoparticle concentration	c_p	specific heat
χ	dimensionless microorganism density	$(\rho c)_f$	effective heat capacity of fluid
η	Similarity variable	ρ	mass density
ξ	Buoyancy parameter	ρc_p	effective heat capacity of the nanoparticle material
$\bar{\theta}_b$	Temperature at the boundary surface	μ	kinematic viscosity
$\bar{\varphi}_b$	nanoparticle concentration at the boundary surface	Lb	bio-convective Lewis number
$\bar{\chi}_b$	motile micro-organisms density at the boundary surface	Pe	bio-convective Peclet number
$\bar{\theta}_{fs}$	Temperatureatfree stream	Ω	Microorganism concentration difference parameter
$\bar{\varphi}_{fs}$	nanoparticle concentration atfree stream	A'''	non-uniform heat source/sink
$\bar{\chi}_{fs}$	motile micro-organisms density) at free stream	A^*	Internal space-dependent heat source/sink.
$D_{\bar{\theta}}$	thermophoresis diffusion coefficient	B^*	Internal temperature-dependent heat source/sink.
ω_c	maximum cell swimming speed	γ	average volume of a microorganism

b	chemotaxis constant	$Sf_{\bar{\xi}}$	Skin friction coefficient
B	Variable magnetic field parameter	$Ht_{\bar{\xi}}$	heat transfer rate
$Re_{\bar{\xi}}$	local Reynolds number	$Ct_{\bar{\xi}}$	nanoparticle transfer rate
$Gr_{\bar{\xi}}$	local Grashof number	$Mt_{\bar{\xi}}$	motile microorganism transfer rate

Author Contributions

Conceptualization: M Trivedi
Methodology: O Otegbeye
Software: SP Goqo
Supervision: Md S Ansari
Validation: Md S Ansari
Writing – original draft: Md S Ansari & M Trivedi
Writing – review & editing: Md S Ansari

References

[1] Srivastava, V. P., Saxena, M., Two-layered model of Casson fluid flow through stenotic blood vessels: applications to the cardiovascular system, *Journal of Biomechanics*, 27(7), 1994, 921-928.

[2] Nadeem, S., UlHaq, R., Lee, C., MHD flow of a Casson fluid over an exponentially shrinking sheet, *Scientia Iranica*, 19(6), 2012, 1550-1553.

[3] Shehzad, S. A., Hayat, T., Qasim, M., Asghar, S., Effects of mass transfer on MHD flow of Casson fluid with chemical reaction and suction, *Brazilian Journal of Chemical Engineering*, 30(1), 2013, 187-195.

[4] Hayat, T., Shehzad, S.A., Alsaedi, A., Alhothuali, M.S., Mixed Convection Stagnation Point Flow of Casson Fluid with Convective Boundary Conditions, *Chinese Physics Letters*, 22(11), 2012, 114704.

[5] Ullah, I., Bhattacharyya, K., Shafie, S., Khan, I., Unsteady MHD mixed convection slip flow of Casson fluid over nonlinearly stretching sheet embedded in a porous medium with chemical reaction, thermal radiation, heat generation/absorption, and convective boundary conditions, *PLoS One*, 11(10), 2016, 135.

[6] Mustafa, M., Hayat, T., Pop, I., Aziz, A., Unsteady boundary layer flow of a Casson fluid due to an impulsively started moving at the plate, *Heat Transfer - Asian Reserach*, 40(6), 2011, 563-576.

[7] Venkatesan, J., Sankar, D. S., Hemalatha, K., Yatim, Y., Mathematical analysis of Casson fluid model for blood rheology in stenosed narrow arteries, *Journal of Applied Mathematics*, 2013, Article ID 583809, 11p.

[8] Zubair, M., Waqas, M, Hayat, T., Ayub, M., Alsaedi. Simulation of nonlinear convectivethixotropic liquid with Cattaneo-Christov heat flux, *Results in Physics*, 22(8), 2018, 1023-1017.

[9] Zubair, M., Waqas, M., Hayat, T., Alsaedi, A., Ayub, M., Stagnation point flow of third-grade liquid due to variable thickness: A useful application to non-Fourier heat flux approach, *Results in Physics*, 8, 2018, 1010-1016.

[10] Zubair, M., Ijaz, M., Abbas, T., Riaz, A., Analysis of modified Fourier law in flow of ferromagnetic Powell-Eyringfluid considering two equal magnetic dipoles, *Canadian Journal of Physics*, 97(7), 2019, 772-776.

[11] Choi, S. U. S., Enhancing thermal conductivity of fluids with nanoparticles, *Proc. 1995 ASME Int. Mech. Eng. Congr. Expo.*, 66, 1995, 99-105.

[12] Eastman, J. A., Choi, S. U. S., Li, S., Yu, W., Thompson, L. J., Anomalously increased effective thermal conductivities of ethylene glycol-based nanofluids containing copper nanoparticles, *Applied Physics Letters*, 78(6), 2001, 718-720.

[13] Hayat, T., Bilal Ashraf, M., Shehzad, S. A., Alsaedi, A., Mixed convection flow of Casson nanofluid over a stretching sheet with convectively heated chemical reaction and heat source/sink, *Journal of Applied Fluid Mechanics*, 8(4), 2015, 803-813.

[14] Anwar, M.I., Tanveer, N., Salleh, M.Z., Shafie, S., Diffusive effects on hydrodynamic Cassonnanofluid boundary layer flow over a stretching surface, *Journal of Physics: Conference Series*, 890, 2017, 1-8.

[15] Sulochana, C., Ashwinkumar, G.P., Sandeep, N., Similarity solution of 3D Casson nanofluid flow over a stretching sheet with convective boundary conditions, *Journal of the Nigerian Mathematical Society*, 35(1), 2016, 128-141.

[16] Madhu, M., Kishan, N., MHD flow and heat transfer of Casson nanofluid over a wedge, *Mechanics & Industry*, 18(2), 2017, 210.

[17] Ahmad, K., Hanouf, Z., Ishak, A., MHD Casson nanofluid flow past a wedge with Newtonian heating, *European Physical Journal Plus*, 132(2), 2017, 87.

[18] Abbas, T., Bhatti, M. M., Ayub, M., Aiding and opposing of mixed convection Cassonnanofluid flow with chemical reactions through a porous Riga plate, *Proc. Inst. Mech. Eng. Part E J. Process Mech. Eng.*, 232(5), 2018, 519-527.

[19] Makinde, O. D., Nagendramma, V., Raju, C. S. K., Leelarathnam, A., Effects of Cattaneo-Christov Heat Flux on Casson Nanofluid Flow Past a Stretching Cylinder, *Defect and Diffusion Forum*, 378, 2017, 28-38.

[20] Ijaz, M., Ayub, M., Zubair, M., Riaz, A., On stratified flow of ferromagnetic nanofluid with heat generation/absorption, *Physica Scripta*, 94(4), 2018, 045206.

[21] Alsabery, A. I., Sheremet, M.A., Chamkha, A.J. and Hashim, I.J.S.R., MHD convective heat transfer in a discretely heated square cavity with conductive inner block using two-phase nanofluid model, *Scientific Reports*, 8(1), 2018, 1-23.

[22] Lu, D, Ramzan, M. Ahmad, S., Chung, J.D. and Farooq, U., A numerical treatment of MHD radiative flow of Micropolar nanofluid with homogeneous-heterogeneous reactions past a nonlinear stretched surface, *Scientific Reports*, 8(1), 2018, 12431.

[23] Sheikholeslami, M., Khan, I., and Tlili, I., Non-equilibrium model for nanofluid free convection inside a porous cavity considering Lorentz forces, *Scientific Reports*, 8(1), 2018, 16881.

[24] Ramzan, M., Sheikholeslami, M., Saeed, M. and Chung, J.D., On the convective heat and zero nanoparticle mass flux conditions in the flow of 3D MHD Couple Stress nanofluid over an exponentially stretched surface, *Scientific Reports*, 9(1), 2019, 562.

[25] Sheikholeslami, M., Shah, Z. Shafee, A. Khan, I. and Tlili, I., Uniform magnetic force impact on water-based nanofluid thermal behavior in a porous enclosure with ellipse-shaped obstacle, *Scientific Reports*, 9(1), 2019, 1196.

[26] Nguyen-Thoi, T., Sheikholeslami, M. Shah, Z., Kumam, P. and Shafee, A., Magnetohydrodynamic nanofluid radiative thermal behavior by means of Darcy law inside a porous media, *Scientific Reports*, 9(1), 2019, 1-11.

[27] Kuznetsov, A. V., The onset of nanofluid bioconvection in a suspension containing both nanoparticles and gyrotactic microorganisms, *International Communications in Heat and Mass Transfer*, 37(10), 2010, 1421-1425.

[28] Platt, J. R., Bioconvection patterns in cultures of free-swimming organisms, *Science*, 133(3466), 1961, 1766-1767.

[29] Sivaraj, R., Animasaun, I. L., Olabiyi, A. S., Saleem, S., Sandeep, N., Gyrotactic microorganisms and thermoelectric effects on the

dynamics of 29nm CuO-water nanofluid over an upper horizontal surface of a paraboloid of revolution, *Multidiscipline Modeling in Materials and Structures*, 14(4), 2018, 695-721.

[30] Kuznetsov, A. V., The onset of thermo-bioconvection in a shallow fluid-saturated porous layer heated from below in a suspension of oxytactic microorganisms, *European Journal of Mechanics - B/Fluids*, 25(2), 2006, 223-233.

[31] Hopkins, M. M., Fauci, L. J., A computational model of the collective fluid dynamics of motile micro-organisms, *Journal of Fluid Mechanics*, 455, 2002, 149-174.

[32] Tarakaramu, N, Narayana, P.V.S., Chemical Reaction Effects on Bio-Convection Nanofluid flow between two Parallel Plates in Rotating System with Variable Viscosity: A numerical study, *Journal of Applied and Computational Mechanics*, 5(4), 2019, 791-803.

[33] Chen, Z., Feng, Q., Liu, R., Chen, J., Ni, F., Development, and application of thermophilic microorganism species in oil recovery, *Acta Petrolei Sinica*, 22(6), 2001, 59-62.

[34] Wu, X., Hou, Z., Shi, M., Wang, Y., Research on using microorganisms to improve chemical flooding effect, *Acta Petrolei Sinica*, 27(1), 2006, 91-94.

[35] Nadeem, S., Khan, M.N., Muhammad, N., Ahmad, S., Mathematical analysis of bio-convectivemicropolar nanofluid, *Journal of Computational Design and Engineering*, 6, 2019, 233-242.

[36] Zilman, G., Novak, J., Liberzon, A., Perkol-Finkel, S., Benayahu, Y., The hydrodynamics of contact of a marine larva, Bugula neritina, with a cylinder, *Journal of Experimental Biology*, 216(15), 2013, 2789-2797.

[37] Khan, W. A., Makinde, O. D., MHD nanofluid bioconvection due to gyrotactic microorganisms over a convectively heat stretching sheet, *International Journal of Thermal Sciences*, 81(1), 2014, 118-124.

[38] Shaw, S., Sibanda, P., Sutradhar, A., Murthy, P. V. S. N., Magnetohydrodynamics and Soret Effects on Bioconvection in a Porous Medium Saturated With a Nanofluid ContainingGyrotactic Microorganisms, *Journal of Heat Transfer*, 136(5), 2014, 052601.

[39] Das, K., Duari, P. R., Kundu, P. K., Nanofluid bioconvection in presence of gyrotactic microorganisms and chemical reaction in a porous medium, *Journal of Mechanical Science and Technology*, 29(11), 2015, 4841-4849.

[40] Makinde O. D., Animasaun, I. L., Thermophoresis and Brownian motion effects on MHDbioconvection of nanofluid with nonlinear thermal radiation and quartic chemical reaction past an upper horizontal surface of a paraboloid of revolution, *Journal of Molecular Liquids*, 221, 2016,733-743.

[41] Latiff, N.A.A., Yahya, E., Ismail, A.I.M., Amirsom, A., Basir, F., The effect of velocity slipand multiple convective boundary conditions in a Darcian porous media with microorganismpast a vertical stretching/shrinking sheet, *AIP Conf. Proc.*, 1870, 2017, 10p.

[42] Alsaedi, A., Khan, M.I., Farooq, M., Gull, N., Hayat, T., Magnetohydrodynamic (MHD) stratified bioconvective flow of nanofluid due to gyrotactic microorganisms, *Advanced Powder Technology*, 28(1), 2017, 288-298.

[43] Aman, F., Khazim, W.N.H.W.M., Mansur, S., Mixed convection flow of a nanofluid containing gyrotactic microorganisms over a stretching/shrinking sheet in the presence of magnetic field, *Journal of Physics: Conference Series*, 890(1), 2017, 11p.

[44] Khan, M.I., Waqas, M., Hayat, T., Khan, M.I., Alsaedi, A., Behaviour of stratification phenomenon in flow of Maxwell nanomaterial with motile gyrotactic microorganisms in the presence of magnetic field, *International Journal of Mechanical Sciences*, 131, 2017, 426-434.

[45] Nagendramma, V., Raju, C.S.K., Mallikarjuna, B., Shehzad, S.A., Leelarathnam, A.,3DCasson nanofluid flow over slendering surface in a suspension of gyrotactic microorganisms with Cattaneo-Christov heat flux, *Applied Mathematics and Mechanics (English Edition)*, 39(5), 2018, 623-638.

[46] Rehman, K.U., Malik, A.A., Tahir, M., Malik, M.Y., Undersized description on motilegyrotactic micro-organisms individualities in MHD stratified water-based Newtonian nanofluid, *Results in Physics*, 8, 2018, 981-987.

[47] Chen, H., Chen, J., Geng, Y., Chen, K., Three-dimensional boundary layer flow over a rotating disk with power-law stretching in a nanofluid containing gyrotactic microorganisms, *Heat Transfer - Asian Research*, 47(3), 2018, 569-582.

[48] Bhatti, M.M., Mishra, S.R., Abbas, T., Rashidi, M.M., A mathematical model of MHDnanofluid flow having gyrotactic microorganisms with thermal radiation and chemical reaction effects, *Neural Computing and Applications*, 30(4), 2018, 1237-1249.

[49] Sulaiman, M., Ali, A., Islam, S., Heat and Mass Transfer in Three-Dimensional Flow of an Oldroyd-B Nanofluid with Gyrotactic Micro-Organisms, *Mathematical Problems in Engineering*, 2018, Article ID 6790420, 1-15.

[50] Rashad, A.M., Chamkha, A.J., Mallikarjuna, B., Abdou, M.M.M., Mixed bioconvection flow of a nanofluid containing gyrotactic microorganisms past a vertical slender cylinder, *Frontiers in Heat and Mass Transfer*, 10, 2018, 21p.

[51] Ramzan, M., Mutaz M., Fares H., Magnetized suspended carbon nanotubes based nanofluid flow with bio-convection and entropy generation past a vertical cone, *Scientific Reports*, 9(1), 2019, 1-15.

[52] Oyelakin, I.S., Mondal, S., Sibanda, P., Nonlinear Radiation in Bioconvective Casson Nanofluid Flow, *International Journal of Applied and Computational Mathematics*, 5, 2019, 124.

[53] Kessler, J.O., Co-operative and concentrative phenomena of swimming micro-organisms, *Contemporary Physics*, 26(2), 1985, 147-166.

[54] Kessler, J.O., Hydrodynamic focusing of motile algal cells, *Nature*, 313(5999), 1985, 218.

[55] Pedley, T.J., Kessler, J.O., Hydrodynamic phenomena in suspensions of swimming microorganisms, *Annual Review of Fluid Mechanics*, 24(1), 1992, 313-358.

[56] Metcalfe, A.M., Pedley, T.J., Falling plumes in bacterial bioconvection, *Journal of Fluid Mechanics*, 445, 2001, 121-149.

[57] Kumar, P.B.S., Gireesha, B.J., Mahanthesh, B., Chamkha, A.J., Thermal analysis of nanofluid flow containing gyrotactic microorganisms in bioconvection and second-order slip with convective condition, *Journal of Thermal Analysis and Calorimetry*, 136, 2019, 19-47.

[58] Khan N.S., Bioconvection in Second Grade Nanofluid Flow Containing Nanoparticles and Gyrotactic Microorganisms, *Brazilian Journal of Physics*, 48(3), 2018, 227-241.

[59] Ali, A., Sulaiman, M., Islam, S., Shah, Z., Bonyah, E., Three-dimensional Magnetohydrodynamic (MHD) flow of Maxwell nanofluid containing gyrotactic micro-organisms with heat source/sink, *AIP Advances*, 8, 2018, 085303.

[60] Atif, S.M., Hussain, S., Sagheer, M., Magnetohydrodynamic stratified bioconvectiveflow of micropolar nanofluid due to gyrotactic microorganisms, *AIP Advances*, 9, 2019, 025208.

[61] Xu, H., Pop, I., Mixed convection flow of a nanofluid over a stretching surface with uniform free stream in the presence of both nanoparticles and gyrotactic microorganisms, *International Journal of Heat and Mass Transfer*, 75, 2014, 610-623.

[62] Ansari, M.S., Motsa S.S., Trivedi, M., Flow and heat transfer of a nanofluid by mixed convection with non-uniform heat source/sink and magnetic field effect: A numerical approach, *Computational Thermal Sciences*, 11(3), 2019, 189-203.

[63] Abbasbandy, S., Ghehsareh, H.R., Solutions of the Magnetohydrodynamic Flow over a nonlinear Stretching Sheet and Nano Boundary Layer over Stretching Surfaces, *International Journal for Numerical Methods in Fluids*, 70, 2012, 1324-1340.

[64] Otegbeye, O., Motsa S.S., Ansari, Md. S., An application of paired quasi-linearization on double-diffusive convection flow over a cone embedded in a porous medium in the presence of nanoparticles, *Heat Transfer-Asian Research*, 48, 2019, 1413-1439.

[65] Trivedi, M., Otegbeye, O., Ansari, M.S., Motsa, S.S., A paired quasi-linearization on magnetohydrodynamic flow and heat transfer

of Casson nanofluid with Hall effects, *Journal of Applied and Computational Mechanics*, 5(5), 2019, 849-860.

[66] Chen, H., Chen, J., Geng, Y., Chen, K., Three-dimensional boundary layer flow over a rotating disk with power-law stretching in a nanofluid containing gyrotactic microorganisms, *Heat Transfer-Asian Research*, 47(3), 2018, 569-582.

ORCID iD

Md.S. Ansari https://orcid.org/0000-0002-9277-0904
O. Otegbeye https://orcid.org/0000-0003-1321-9776
M. Trivedi https://orcid.org/0000-0003-2575-4004
S.P. Goqo https://orcid.org/0000-0003-1383-068X